PHYSICAL REVIEW D

PARTICLES AND FIELDS

THIRD SERIES, VOL. 5, NO. 3 1 February 1972

$\pi^{\pm}$-Proton Elastic Scattering at 180° from 0.60 to 1.60 GeV/c†

R. E. Rothschild, T. Bowen, P. K. Caldwell,* D. Davidson, E. W. Jenkins, R. M. Kalbach, D. V. Petersen, and A. E. Pifer

Department of Physics, University of Arizona, Tucson, Arizona 85721

(Received 17 June 1971)

The differential cross section for $\pi^{\pm}$-p elastic scattering at 180° was measured from 0.572 to 1.628 GeV/c using a double-arm scintillation-counter spectrometer with an angular acceptance θ^* in the center-of-mass system defined by $-1.00 \leq \cos\theta^* \leq -0.9992$. The π^+-p cross section exhibits a large dip at 0.737 GeV/c and a broad peak centered near 1.31 GeV/c. The π^--p cross section exhibits peaks at 0.69, 0.97, and 1.43 GeV/c.

We report here the results of a determination of $\pi^{\pm}$-p elastic, differential cross sections at 180° in the momentum range 0.572–1.628 GeV/c using a double-arm counter spectrometer. Measurements were made at intervals of incident momentum which varied from 18 to 40 MeV/c, with typical statistical errors in the cross section of a few percent and with an over-all normalization error which is estimated to be less than ±5.3%. Structure observed in the momentum dependence of the cross sections in this region provides a new test of current parametrizations of phase-shift analysis and resonance models.

The experiment was performed at the Lawrence Radiation Laboratory Bevatron using the configuration of counters and magnets shown in Fig. 1. The secondary pion beam came to a final focus 10 ft downstream from the hydrogen target and had a momentum spread $\Delta p/p$ of not more than ±0.75%, a solid-angle acceptance of 2.4×10^{-3} sr, and an intensity which varied from 10 000 to 300 000 pions per 4×10^{10} protons on the primary target. A typical absolute pion intensity was 100 000 pions per accelerator pulse of 0.5-sec duration. The spatial extent of the beam, measured at the downstream end of the hydrogen target flask, was typically 2 in. in the horizontal and 1.5 in. in the vertical direction.

Incident beam pions were selected by four scintillation counters (S_1, S_2, $\bar{G}$, and S_3), a Plexiglas Čerenkov counter (C_0), and a high-pressure gas Čerenkov counter ($\bar{C}_1$). The 32.1-ft flight path between S_1 and S_2, located downstream from C_0, and S_3, located at the upstream end of the hydrogen target, was used to reject protons and kaons by time-of-flight differences. C_0 was operated as a threshold detector to provide further rejection of protons and kaons in the incident beam. Electrons and positrons accompanying beam pions were rejected by a factor of 50:1 by the high-pressure Čerenkov counter $\bar{C}_1$ which was operated at 65 psia of carbon dioxide. Correction for muon contamination and determination of thresholds for pions and muons was obtained from curves of counting rate versus pressure for $\bar{C}_1$ made during the tuning phase of the experiment.

The beam momentum was determined by measuring the differences in time of flight for pions and protons along the 32.1-ft flight path and correcting for the momentum loss of pions and protons in the remainder of the incident beam path. The error in such measurements was estimated to be ±0.5%.

The liquid-hydrogen target flask was 6 in. in diameter and 12 in. in length, with convex Mylar end

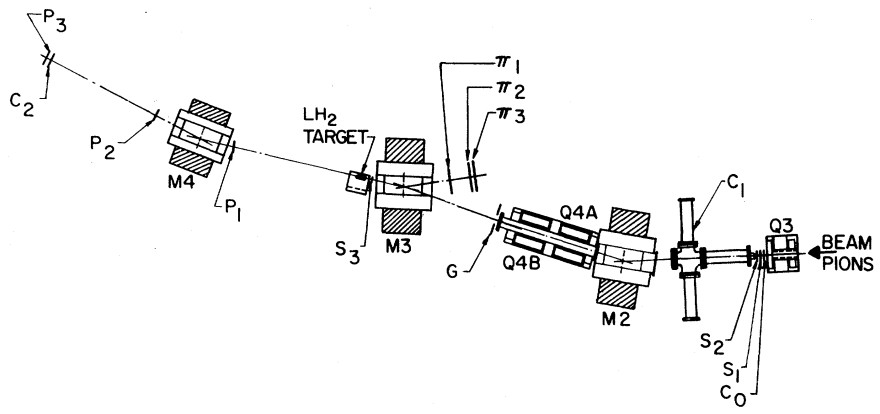

FIG. 1. Experimental configuration of counters and magnets using a secondary pion beam from the Lawrence Radiation Laboratory Bevatron.

caps. Its effective length was determined by measuring the profile of these caps at liquid-nitrogen temperature and averaging its length over the measured spatial distribution of the incident pion beam. The target flask and an identical but empty flask could be remotely positioned by means of a pneumatic device in order to place either one on the beam axis for a periodic check of background during the experimental runs.

Elastically scattered pions and recoil protons were detected by the pion and proton arms of a double-arm spectrometer, each arm of which contained counters and a bending magnet. The angular resolutions of the proton and pion arms were ±1.3° and ±5.5°, respectively, with respective momentum resolutions of ±9.3% and ±35.5%. When combined with fast timing, this momentum analysis provided additional discrimination against inelastic events. The time delay between the incident pion as it traverses S_3 and the recoil proton as it traverses P_3, a flight path of 26.6 ft, was displayed in a pulse-height analyzer (PHA) with a time resolution of 0.75 nsec for individual events.

The pion arm consisted of three scintillation counters (π_1, π_2, and π_3), rigidly attached to a movable framework, and a bending magnet (M3) which deflected scattered pions away from the incident beam. The proton arm consisted of scintillation counters (P_1, P_2, and P_3), a Čerenkov counter ($\bar{C}_2$), and a bending magnet (M4) positioned approximately 3 ft downstream from the final focus. For a negative-pion beam, M4 deflected beam particles away from P_2, $\bar{C}_2$, and P_3 to eliminate contamination from this source. However, for a positive-pion beam above 1.0-GeV/c incident momentum, beam pions and recoil protons were separated by less than the radius of counter P_3. In this case a Plexiglas Čerenkov counter ($\bar{C}_2$) was employed to discriminate against beam pions.

In order to reduce relative systematic errors from one datum to the next, the apparatus was designed so as to minimize changes in the experimental configuration during the course of the experiment. The only change required when the incident momentum was changed by 20 MeV/c was an angular shift of about 0.2° in the position of the scattered-pion telescope.

The electronics circuitry made use of the technique of providing two separate 200-MHz discriminators for certain counters, one set at a low threshold level to provide jitter-free, leading-edge timing signals (called "fast") and the other set at a high threshold to provide a high level of discrimination against background signals (called "slow"). Coincidence outputs signaling the presence of beam particles, recoil protons, and scattered pions were designated π, P_{123}, and π_{123}, respectively.

The π coincidence output was formed from the combination $\pi = S_1S_2S_3C_0\bar{C}_1\bar{G}$, with provision for vetoing this output in the event that two beam particles were separated in time by less than 20 nsec. A π coincidence output signaled that a single pion (or occasionally a muon) was about to enter the hydrogen target, the timing of this output being determined by S_3(fast).

The P_{123} coincidence output was formed from the combination $P_{123} = P_1P_2P_3\bar{C}_2$ for positive incident beam and $P_1P_2P_3$ for a negative beam. Timing of this output was determined by P_3(fast). A coincidence was also formed from π and P_{123} outputs, called πP, with appropriate delays to account for particle flight times.

A similar coincidence, $\pi\pi$, was formed between the π and π_{123} outputs to detect the presence of beam and scattered pions with a delay appropriate for the flight paths involved. An "event" output signal was then determined by a coincidence between πP and $\pi\pi$, the timing of which was governed

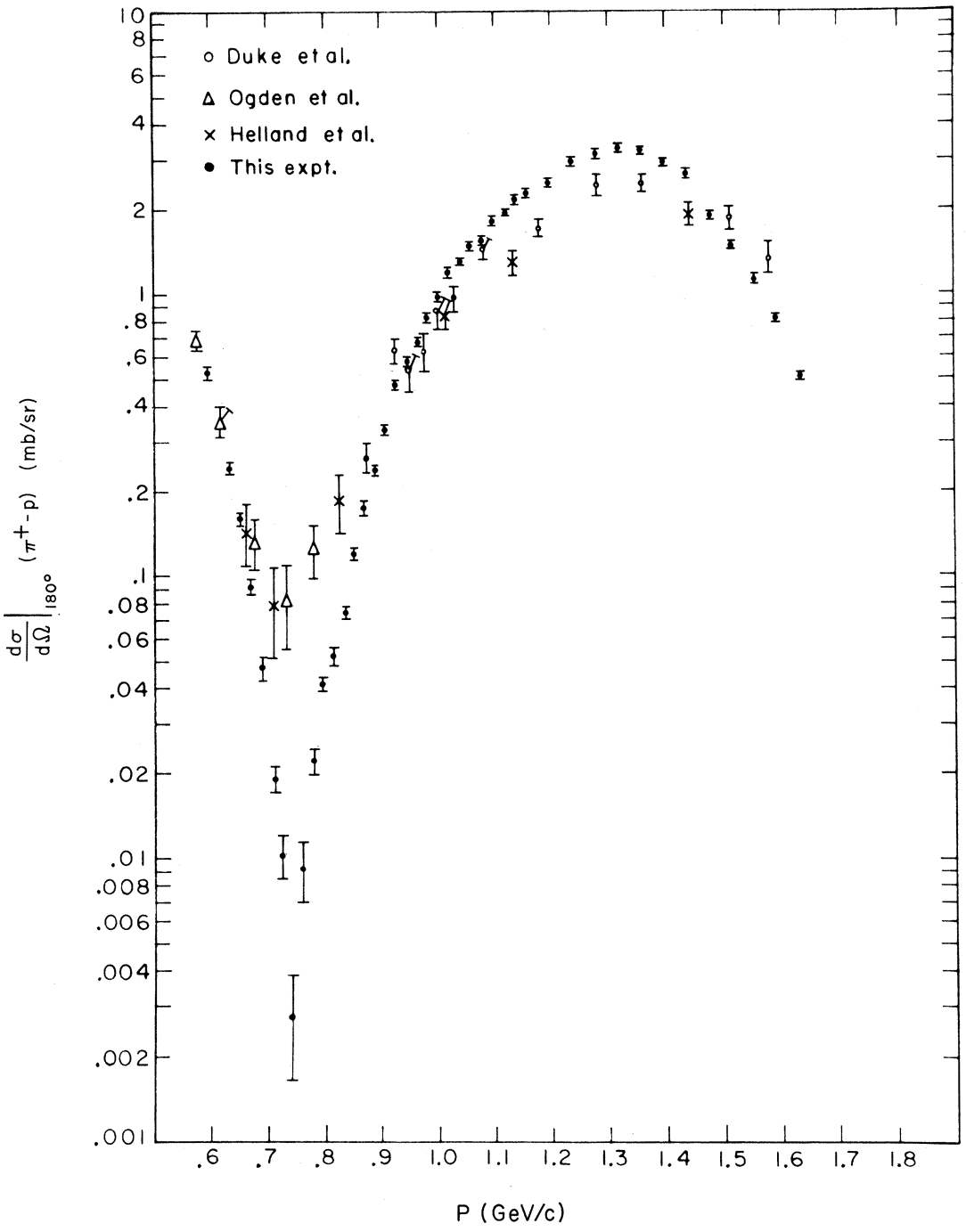

FIG. 2. Elastic differential cross section at 180° for π^+-proton scattering together with the results of other experiments near 180°. The symbols correspond to the following references: ○, Ref. 1; △, Ref. 2; ×, Ref. 3; ●, present experiment.

by P_3(fast). The PHA was used to display the distribution of times between the output of "event" and the output of π which corresponded to the distribution of flight times for the recoil proton over the 26.6-ft flight path from the hydrogen target to P_3 and therefore provided additional information for background subtraction.

The 180° differential cross section is given by

$$\left(\frac{d\sigma}{d\Omega}\right)_{180°} = K\left(\frac{N_F - N_E}{N_B}\right) \times \frac{w}{A\rho L} \times \frac{1}{E\Delta\Omega^*},$$

where K is a correction factor, N_F is the number

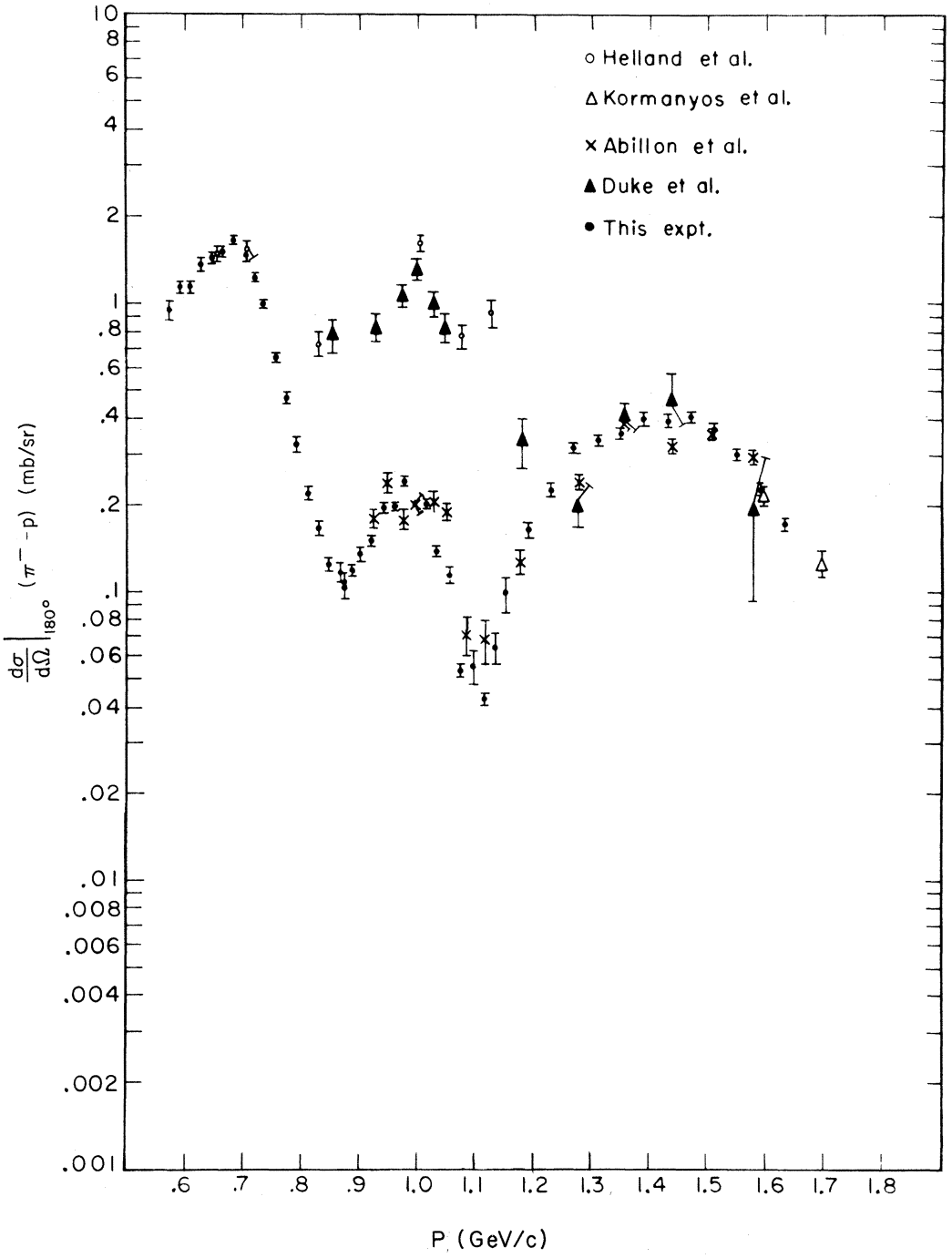

FIG. 3. Elastic differential cross section at 180° for π^- -proton scattering together with the results of other experiments near 180°. The symbols correspond to the following references: ○, Ref. 3; △, Ref. 4; ×, Ref. 5; ▲, Ref. 1; ●, present experiment.

of full-target events, N_E is the corresponding number of empty-target events, N_B is the number of beam pions which strike the full target, w is the gram molecular weight of hydrogen, A is Avogadro's number, ρ is the density of liquid hydrogen, taken as 0.0708 g/cm^3, L is the effective target length (11.91 ± 0.06 in.), and $E\Delta\Omega^*$ is the effective-efficiency–solid-angle product for the double-arm spectrometer.

Corrections included in K involve factors related

to counter efficiences, finite counter sizes, pion decay, muon contamination, and nuclear absorption by liquid hydrogen, counters, and air. While some of these corrections remained fixed over the momentum range covered, others were strongly momentum-dependent. Typical percentage corrections due to these sources together with their corresponding uncertainties are as follows: counter inefficiencies, $(6.5 \pm 2.5)\%$; counter size, $(3.0 \pm 0.1)\%$; nuclear absorption of protons in liquid hydrogen, $(2.0 \pm 0.1)\%$; scattered negative pions in liquid hydrogen, $(3.5 \pm 0.1)\%$; scattered positive pions in liquid hydrogen, $(10.0 \pm 0.1)\%$; recoil protons in counters, $(1.5 \pm 0.2)\%$; scattered negative pions in counters, $(1.0 \pm 0.2)\%$; scattered positive pions in counters, $(2.5 \pm 0.2)\%$; attentuation of protons and positive pions by air, $(0.75 \pm 0.1)\%$, and of negative pions by air, $(0.25 \pm 0.1)\%$; decay of scattered pions in flight, $(10.0 \pm 0.2)\%$; incident pion decay or absorption in the region from S_3 to the center of the hydrogen target, $(3.0 \pm 0.1)\%$; and

TABLE I. π^+-p 180° elastic differential cross sections.

Momentum (GeV/c)	$E\Delta\Omega^*$ (msr)	$1/K$	$d\sigma/d\Omega$ (mb/sr)	Error (mb/sr)
0.592	5.02	0.667	0.533	0.025
0.610	4.98	0.664	0.384	0.021
0.628	4.95	0.661	0.245	0.010
0.646	4.91	0.658	0.161	0.009
0.664	4.87	0.656	0.092 2	0.006 1
0.683	4.82	0.654	0.047 1	0.004 5
0.701	4.79	0.651	0.019 1	0.002 0
0.719	4.73	0.649	0.010 3	0.001 8
0.737	4.68	0.649	0.002 76	0.001 10
0.756	4.63	0.647	0.009 25	0.002 24
0.774	4.58	0.645	0.022 1	0.002 3
0.792	4.51	0.644	0.041 3	0.002 6
0.811	4.46	0.642	0.052 1	0.003 8
0.829	4.40	0.642	0.074 3	0.003 7
0.847	4.36	0.640	0.121	0.006
0.866	4.31	0.638	0.176	0.011
0.883	4.26	0.637	0.240	0.008
0.901	4.21	0.637	0.331	0.010
0.920	4.17	0.639	0.481	0.013
0.939	4.12	0.638	0.582	0.020
0.958	4.07	0.637	0.688	0.011
0.977	4.03	0.638	0.836	0.024
0.996	3.99	0.637	0.977	0.012
1.015	3.95	0.638	1.197	0.034
1.034	3.90	0.639	1.320	0.018
1.053	3.86	0.637	1.489	0.033
1.073	3.82	0.639	1.575	0.024
1.092	3.78	0.639	1.805	0.042
1.113	3.74	0.639	1.953	0.028
1.130	3.71	0.639	2.144	0.044
1.150	3.67	0.639	2.261	0.027
1.189	3.59	0.639	2.475	0.051
1.229	3.52	0.640	2.991	0.059
1.269	3.44	0.639	3.140	0.063
1.309	3.37	0.639	3.314	0.065
1.349	3.30	0.639	3.263	0.048
1.389	3.23	0.639	2.932	0.062
1.438	3.17	0.641	2.669	0.056
1.468	3.11	0.643	1.903	0.032
1.508	3.06	0.643	1.487	0.030
1.548	3.01	0.644	1.131	0.022
1.588	2.96	0.645	0.820	0.022
1.628	2.91	0.645	0.510	0.023

TABLE II. π^--p 180° elastic differential cross sections.

Momentum (GeV/c)	$E\Delta\Omega^*$ (msr)	$1/K$	$d\sigma/d\Omega$ (mb/sr)	Error (mb/sr)
0.572	5.05	0.740	0.939	0.068
0.592	5.02	0.739	1.127	0.046
0.610	4.98	0.739	1.126	0.046
0.628	4.95	0.737	1.365	0.079
0.646	4.91	0.736	1.429	0.053
0.664	4.87	0.733	1.513	0.047
0.683	4.82	0.733	1.646	0.055
0.701	4.79	0.730	1.444	0.047
0.719	4.73	0.733	1.221	0.041
0.737	4.68	0.734	0.986	0.031
0.756	4.63	0.734	0.654	0.030
0.774	4.58	0.735	0.467	0.024
0.792	4.51	0.735	0.324	0.019
0.811	4.46	0.735	0.217	0.010
0.829	4.40	0.734	0.164	0.008
0.847	4.36	0.734	0.124	0.007
0.866	4.31	0.731	0.117	0.010
0.883	4.26	0.729	0.118	0.005
0.901	4.21	0.727	0.134	0.008
0.920	4.17	0.726	0.151	0.009
0.939	4.12	0.724	0.195	0.008
0.958	4.07	0.723	0.197	0.005
0.977	4.03	0.724	0.244	0.008
0.996	3.99	0.725	0.202	0.005
1.015	3.95	0.729	0.200	0.006
1.034	3.90	0.731	0.137	0.004
1.053	3.86	0.733	0.115	0.008
1.073	3.82	0.735	0.0530	0.0026
1.092	3.78	0.737	0.0553	0.0075
1.113	3.74	0.738	0.0427	0.0024
1.130	3.71	0.740	0.0639	0.0077
1.150	3.67	0.741	0.0989	0.0145
1.189	3.59	0.742	0.164	0.013
1.229	3.52	0.743	0.227	0.013
1.269	3.44	0.744	0.314	0.015
1.309	3.37	0.745	0.334	0.017
1.349	3.30	0.746	0.356	0.017
1.389	3.23	0.748	0.396	0.021
1.438	3.17	0.749	0.392	0.014
1.468	3.11	0.751	0.402	0.015
1.508	3.06	0.752	0.363	0.017
1.548	3.01	0.754	0.301	0.013
1.588	2.96	0.754	0.225	0.014
1.628	2.91	0.755	0.172	0.009

contamination due to muons in the incident beam, $(3.0 \pm 0.5)\%$.

The factor $(N_F - N_E)/N_B$ was determined from the PHA distributions which, when combined with scaler readings, permitted a detailed analysis of various types of background. It was determined after examination of flight times that a time interval of 8 nsec in the PHA distributions was sufficient to include 99.6% of the recoil-proton flight times. N_E included corrections for accidental coincidences, interactions in the hydrogen and the Mylar windows of the target, and inelastic and quasi-elastic events.

A Monte Carlo calculation of the acceptance of the system for inelastic events in which a single π^0 is created gave 10^{-3} relative to the acceptance for elastic events, a result consistent with the generally low backgrounds obtained.

The factor $E\Delta\Omega^* = \int E(\Omega^*)\, d\Omega^*$ is the efficiency–solid-angle product, where $E(\Omega^*)$ is the probability that a pion scattered into the solid angle Ω^* will strike all pion counters and the recoil proton will strike all proton counters. A Monte Carlo calculation showed a variation of $E(\Omega^*)$ with $\cos\theta^*$ which was a maximum for $\cos\theta^* = -1$ and which fell to half this value for $\cos\theta^*$ ranging from -0.9992 to -0.9996, depending upon momentum.

The results of the 180° cross-section measurement are shown in Figs. 2 and 3, together with some previous results, and listed in Tables I and II, the errors listed being statistical only. Overall normalization error is estimated to be less than $\pm 5.3\%$.

For the π^+-p cross section we note general qualitative agreement with previous results in several intervals of the momentum region covered. However, the relatively small angular acceptance at 180° of the present experiment and the resulting reduction of the spin-flip contribution to the results is presumed to be responsible for the observed enhancement of the dip at 0.737 GeV/c relative to previous results such as those of Ogden *et al.*[2] taken at θ^* in the region 160°–165°.

For the π^-p cross section the results show peaks at 0.69, 0.98, and 1.44 GeV/c and are in general agreement with previous results. However, in the region 0.775–1.25 GeV/c the present results are lower than those obtained previously by Duke *et al.*[1] and Helland *et al.*,[3] presumably owing again to the relatively small angular acceptance at 180° of the present experiment.

A comparison with predictions of phase-shift analysis[6] gives the best agreement for the Glasgow B parameter set, but, in general, the results are smoother than the phase-shift predictions. In particular, all the Berkeley fits exhibit structure not observed, and the CERN Experimental and the Kirsopp fits contain several unobserved dips and peaks, although they are in general agreement for the positive-pion results. The CERN Theoretical and the Saclay results give a good fit to the positive-pion data but not to the negative-pion data.

A comparison with current predictions using resonance models shows varying degrees of success in certain regions of the π^+ and π^- data, with no single model giving a good over-all fit to the data in the momentum range of the present experiment. Comparison with the model proposed by Shanta[7] shows good agreement with the shapes and positions of the peaks and dips for the positive data, but the predictions for the negative data fail to reproduce the peak at 0.98 GeV/c. Carroll *et al.*[8] devised a model which gives a reasonably good qualitative fit to both the positive- and negative-pion results, but which gives relatively poor agreement with the observed ratios of peak-to-dip values for the cross section over the momentum range of the present results.

We gratefully acknowledge the members of the Bevatron staff and crew, in particular W. Hartsough, for their cooperation and hospitality, and T. Elioff for his advice and encouragement.

---

†Research supported by a grant from the National Science Foundation. Based upon a thesis submitted (by R. E. R.) in partial fulfillment of the requirements for the Ph.D. degree.

*Present address: Department of Physics, University of Michigan, Ann Arbor, Mich. 48104.

[1]P. J. Duke, D. P. Jones, M. A. R. Kemp, P. G. Murphy, J. D. Prentice, and J. J. Tresher, Phys. Rev. 149, 1077 (1966).

[2]P. M. Ogden, D. E. Hagge, J. A. Helland, M. Banner, J. F. Detoeuf, and J. Teiger, Phys. Rev. 137, B1115 (1965).

[3]J. A. Helland, T. J. Devlin, D. E. Hagge, M. J. Longo, B. J. Moyer, and C. D. Wood, Phys. Rev. 134, B1062 (1964); J. A. Helland, C. D. Wood, T. J. Devlin, D. E. Hagge, M. J. Longo, B. J. Moyer, and V. Perez-Mendez, *ibid.* 134, B1079 (1964).

[4]S. W. Kormanyos, A. D. Krisch, J. R. O'Fallon, K. Ruddick, and L. G. Ratner, Phys. Rev. Letters 16, 706 (1966).

[5]J. M. Abillon, A. Borg, M. Crozon, T. Leray, J. P. Mendiburu, and J. Tocqueville, Phys. Letters 32B, 712 (1970).

[6]Particle Data Group, University of California Radia-

tion Laboratory Report No. UCRL-20030πN, 1970 (unpublished).
[7]R. Shanta, Nuovo Cimento 70A, 12 (1970).
[8]A. S. Carroll, J. Fischer, A. Lundby, R. H. Phillips, C. L. Wang, F. Lobkowicz, A. C. Melissinos, Y. Nagashima, and S. Tewksbury, Phys. Rev. Letters 20, 607 (1968).

PHYSICAL REVIEW D VOLUME 5, NUMBER 3 1 FEBRUARY 1972

Coherent K^+d Interactions at 12 GeV/c*

A. Firestone,† G. Goldhaber, D. Lissauer, and G. H. Trilling
Department of Physics and Lawrence Berkeley Laboratory, University of California, Berkeley, California 94720

(Received 18 October 1971)

We have made a study of the coherent reactions $K^+d \to K^+\pi^+\pi^-d$ and $K^+d \to K^0\pi^+d$ at 12 GeV/c, using data obtained in the SLAC 82-in. bubble chamber. The cross sections for these two processes are 331 ± 35 and 19 ± 4 μb, respectively. The reaction $K^+d \to K^+\pi^+\pi^-d$ is dominated by Q production in the $K\pi\pi$ system. The shape of the Q enhancement is nearly identical to that observed in the reaction $K^+p \to K^+\pi^+\pi^-p$ at similar energies. This result may be interpreted in terms of mixing between the strange members of the A_1 and B nonets. There are also an L signal at $M(K\pi\pi) \sim 1.72$ GeV and a d^* signal at $M(d\pi^+) \sim 2.2$ GeV. The L appears to be formed primarily in conjunction with the d^*, with the π^+ meson shared between the two of them. The reaction $K^+d \to K^0\pi^+d$ is dominated completely by $K^*(890)$ production.

I. INTRODUCTION

In this paper we present an analysis of the coherent reactions $K^+d \to K^+\pi^+\pi^-d$ and $K^+d \to K^0\pi^+d$ at 12 GeV/c, from data obtained with the SLAC 82-in. deuterium-filled bubble chamber. These reactions, in which the deuteron emerges intact in the final state, are particularly interesting in that the coherence acts as a filter in allowing only $I=0$ non-spin-flip exchange at the deuteron vertex.

It has been suggested that the Q, as produced in hydrogen, for example in the reaction $K^+p \to K^+\pi^+\pi^-p$, has both $J^{PC}=1^{++}$ and 1^{+-} components, where C is the charge-conjugation quantum number of the neutral nonstrange members of the same nonet ($C=+1$ for the A_1 nonet and $C=-1$ for the B nonet).[1-3] Since the strange mesons are not eigenstates of C, a generalization of C called "unitary parity" has been introduced by Dothan, which is expected to hold for each entire nonet.[4] A particularly straightforward interpretation for two distinct $J^P=1^+$ states is obtained from the quark model where the A_1 and B nonets are considered as the $^3P_1$ and $^1P_1$ $q\bar{q}$ states.[5]

Experimentally the evidence[6,7] that the Q enhancement consists of (at least) two distinct $J^P=1^+$ states appears rather well established by now[8,9]: the Q_A at $M \approx 1.25$ GeV and Q_B at $M \approx 1.38$ GeV. The lower-mass state Q_A may be the same object as the $C(1240)$ meson observed in nondiffractive reactions.[10]

Two overlapping $J^P=1^+$ K^* states, which decay into the same final state $K\pi\pi$, may give rise to new phenomena. The states can mix[1] so that the physical states Q_A and Q_B are mixtures of the intrinsic states K_A and K_B belonging to the two distinct nonets. Thus one can define a mixing angle φ such that[11]

$$Q_A = K_A \cos\varphi + K_B \sin\varphi,$$

$$Q_B = -K_A \sin\varphi + K_B \cos\varphi .$$

Furthermore, interference effects between the physical states Q_A and Q_B may also be present.[2] In the absence of mixing between these two components of the Q (exact SU_3 symmetry), and with the assumption of Pomeranchukon exchange, the $J^{PC}=1^{+-}$ component of the Q (i.e., Q_B) is expected to vanish in the coherent reaction in deuterium. Conversely, the presence of Q_B in coherent production can be interpreted as evidence for the above-mentioned K^* mixing effect. The work reported here includes the results of a search for these mixing effects, as well as a study of L and d^* production.

In Sec. II we discuss the beam, scanning, measuring, and separation techniques which were used to obtain the data sample of $K^+d \to K^+\pi^+\pi^-d$ events. In addition, ambiguity problems and our methods of handling them are discussed at length. In Sec. III we describe the general features of the reaction, and the cross-section determination is given. In Sec. IV the physics of the d^* enhancement is presented, and in Sec. V the L-meson data are discussed. Section VI deals with the Q enhancement and treats production mechanisms as well as decay properties. Section VII deals briefly with the companion coherent reaction $K^+d \to K^0\pi^+d$, and Sec. VIII presents the main conclusions of this study.